Supporting Information

Elucidating the Failure Mechanisms of Perovskite Solar Cells in Humid Environments Using *In Situ* Grazing-Incidence Wide Angle X-ray Scattering

*Kyle M. Fransishyn, Soumya Kundu, and Timothy L. Kelly**

Department of Chemistry, University of Saskatchewan, 110 Science Place, Saskatoon, Saskatchewan S7N 5C9, Canada

EXPERIMENTAL METHODS

Materials. Both methylammonium iodide[1] and a ZnO nanoparticle suspension (6 mg·mL^{-1} in 1-butanol)[2] were prepared according to established literature procedures. Lead(II) iodide (99%), lithium bis(trifluoromethanesulfonyl)imide (Li-TFSI, 99%), 4-*tert*-butylpyridine (96%), and titanium diisopropoxide bis(acetylacetonate) (75% w/w in isopropanol) were purchased from Millipore Sigma. Poly(3-hexylthiophene) (P3HT, electronic grade) was purchased from Rieke Metals. Ag (99.99%) and Au (99.99%) pellets were purchased from Kurt J. Lesker. ITO-coated glass (25 mm × 25 mm × 1.1 mm, R_s = 15-25 Ω/□) and FTO-coated glass (300 mm × 300 mm × 3.3 mm, R_s = 7 Ω/□) were purchased from Delta Technologies and Millipore Sigma, respectively; the FTO-coated glass was cut to size (25 mm × 25 mm) prior to use. All other chemicals were purchased from Fisher Scientific and used as-received.

Cell fabrication. ITO-glass substrates were cleaned by sequential sonication for 20 min in each of a detergent solution (2% v/v Extran 300), acetone, and isopropanol, then stored under isopropanol. Immediately prior to use, the substrates were blown dry in a stream of nitrogen and subjected to 30 min of UV/ozone cleaning. A ZnO electron-transport layer was deposited by spin coating (500 r.p.m. for 3 s, followed by 3000 r.p.m. for 25 s) from a nanoparticle solution (6 mg·mL^{-1} in 1-butanol); the process was repeated three times to build up the desired ZnO layer thickness. The samples were then stored in a nitrogen-filled glovebox (~ 1 ppm H_2O and O_2) until use. A 130 nm layer of PbI_2 was deposited by thermal evaporation at a base pressure of 1 × 10^{-6} mbar. The films were then transferred to a humidity-controlled glove bag (RH = 40%) containing a spin coater. While in the glove bag, the films were immersed in a solution of CH_3NH_3I in isopropanol (10 mg/mL) for 2 min, then spun at 3000 r.p.m. for 20 s to dry. The process was repeated three times in order to convert all of the PbI_2 into $CH_3NH_3PbI_3$. The films were removed from the glove bag after 5 min. A P3HT solution (20 mg P3HT, 3.4 μL of 4-*tert*-butylpyridine, and 6.4 μL of Li-TFSI solution (28 mg Li-TFSI dissolved in 1 mL of acetonitrile), all dissolved in 1 mL of chlorobenzene) was spin coated (1000 r.p.m. for 25 s) onto the perovskite films. The partially-finished

device was returned to the glovebox, and a top electrode (either Ag or Au) deposited by thermal evaporation at a base pressure of 1×10^{-6} mbar. The approximate cell area was ~ 0.13 cm^2.

Cell characterization. Cell performance was measured inside a nitrogen-filled glovebox (~ 1 ppm H_2O and O_2). The devices were illuminated with a 450 W Class AAA solar simulator (Sol3A, Newport) equipped with an AM1.5G filter. The illumination intensity was calibrated to 1 Sun using a silicon reference cell (91150V, Newport), and the cell area was defined to be 0.101 cm^2 using a non-reflective black anodized aluminum aperture mask. *J-V* curves were obtained with a Keithley 2400 source-measure unit. Prior to acquisition, the cells were light soaked for 5 s. The voltage was swept from forward bias toward short-circuit (1.2 V to −0.1 V) in 100 steps with a 50 ms dwell time at each step. The cells displayed only a small amount of hysteresis in the *J-V* curves, as described in our previous work.[3]

GIWAXS. GIWAXS measurements were performed at the Hard X-ray MicroAnalysis (HXMA) beamline of the Canadian Light Source. An energy of 17.998 keV (λ = 0.6888 A) was selected using a Si(111) monochromator. The diffraction patterns were collected on a SX165 CCD camera (Rayonix) using an acquisition time of 3 s (unless otherwise stated). The sample-to-detector distance (272 mm) was calibrated using a LaB_6 powder standard.

For *in situ* experiments, devices were mounted in a gas-tight sample chamber (Figure S2). Nitrogen carrier gas was connected to a series of mass flow controllers (Alicat MC-5SLPM-D) and water-filled bubblers, and the output of this system connected to the sample chamber (Figure 1). The relative humidity inside the chamber was controlled by varying the relative flow rates of dry nitrogen and nitrogen saturated with water vapor, and was validated by a flange-mounted humidity sensor (RH-USB, Omega). The beam from a halogen fiber optic illuminator (Fiber-Lite, MI-150) was reflected upward by a 45° silver mirror (BBSO1-E02, Thor Labs) in order to illuminate the cells from below. A Keithley 2634B source-measure unit was used to acquire *I-V* curves at 60 s intervals; GIWAXS patterns were acquired every 180 s. A high output LED light source (MityCross, Cygo-Lite) was used to compare the effect of spectral output on the perovskite degradation pathway. The output spectra of the halogen illuminator and LED source were

measured with a USB 2000+ spectrophotometer (Ocean Optics), which had a 600 line grating blazed at 400 nm, leading to an effective bandwidth of 200 – 800 nm.

Data processing. The 2D GIWAXS patterns were processed using the GIXSGUI[4] software package; the patterns were calibrated, solid angle corrections applied, and the data reshaped to account for the missing wedge along q_z. Azimuthally-integrated scattering intensities were calculated using the Datasqueeze 3.0 software package; data were azimuthally-integrated between $-75° \leq \chi \leq 75°$ and $0.3\ \text{Å}^{-1} \leq q \leq 2.9\ \text{Å}^{-1}$ in $0.002\ \text{Å}^{-1}$ increments. In order to compensate for the loss of ring current over the course of the experiment, the intensity was normalized to the Au (111) reflection at $q = 2.66\ \text{Å}^{-1}$, which was assumed to be invariant over the course of the experiment. The diffuse background (primarily due to scattering from the glass substrate) was subtracted by fitting to a spline curve. The FWHM of the (110) scattering peak was calculated by fitting the peak to a Gaussian function.

Table S1. Average device parameters for the ITO/ZnO/$CH_3NH_3PbI_3$/P3HT/Ag cells prepared in this study.

J_{sc} (mA/cm^2)	V_{oc} (V)	FF	PCE (%)
14.7 ± 0.9	0.95 ± 0.03	0.62 ± 0.04	8.7 ± 0.6

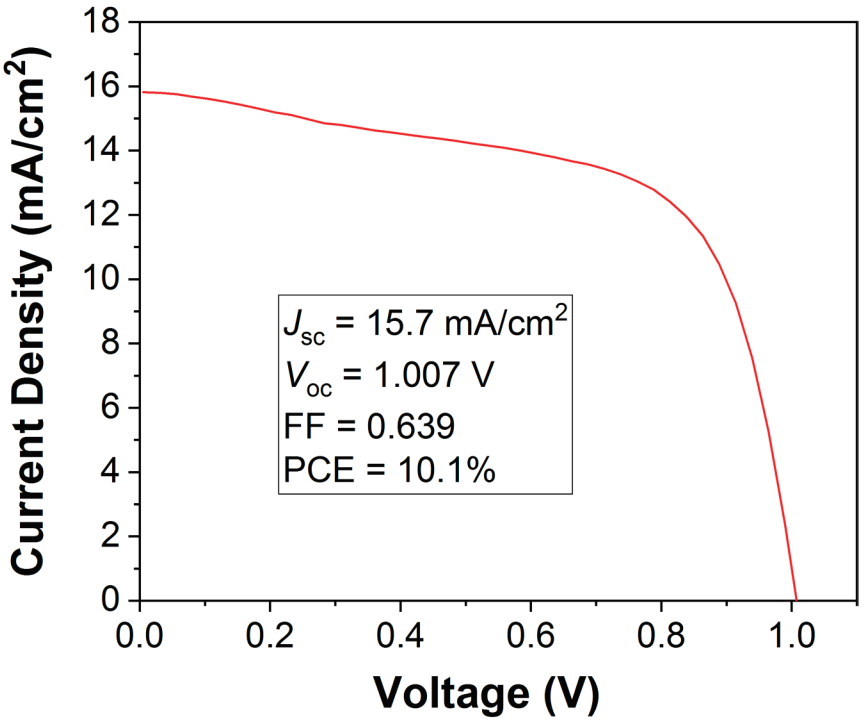

Figure S1. *J-V* curve of the champion ITO/ZnO/$CH_3NH_3PbI_3$/P3HT/Ag cell from this study.

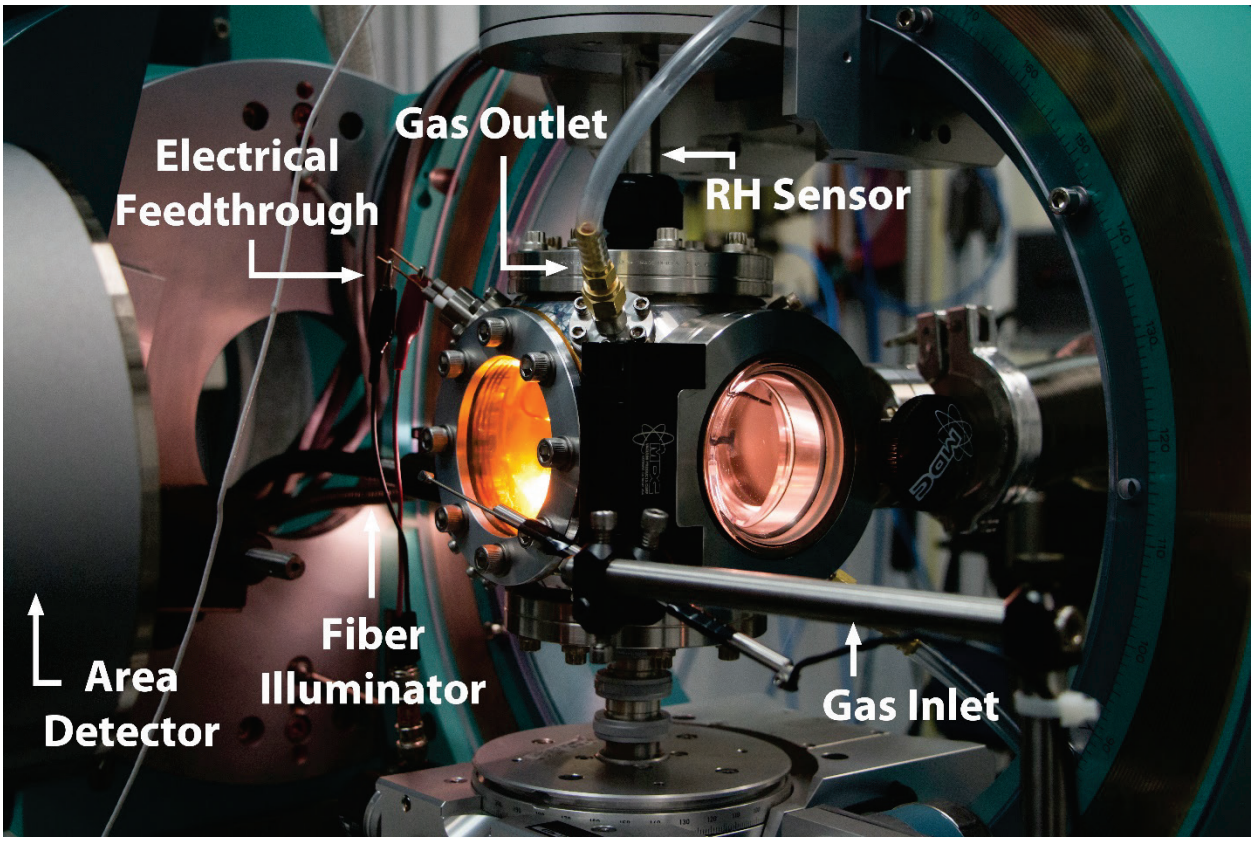

Figure S2. Photograph of the *in situ* sample chamber mounted at the HXMA beamline.

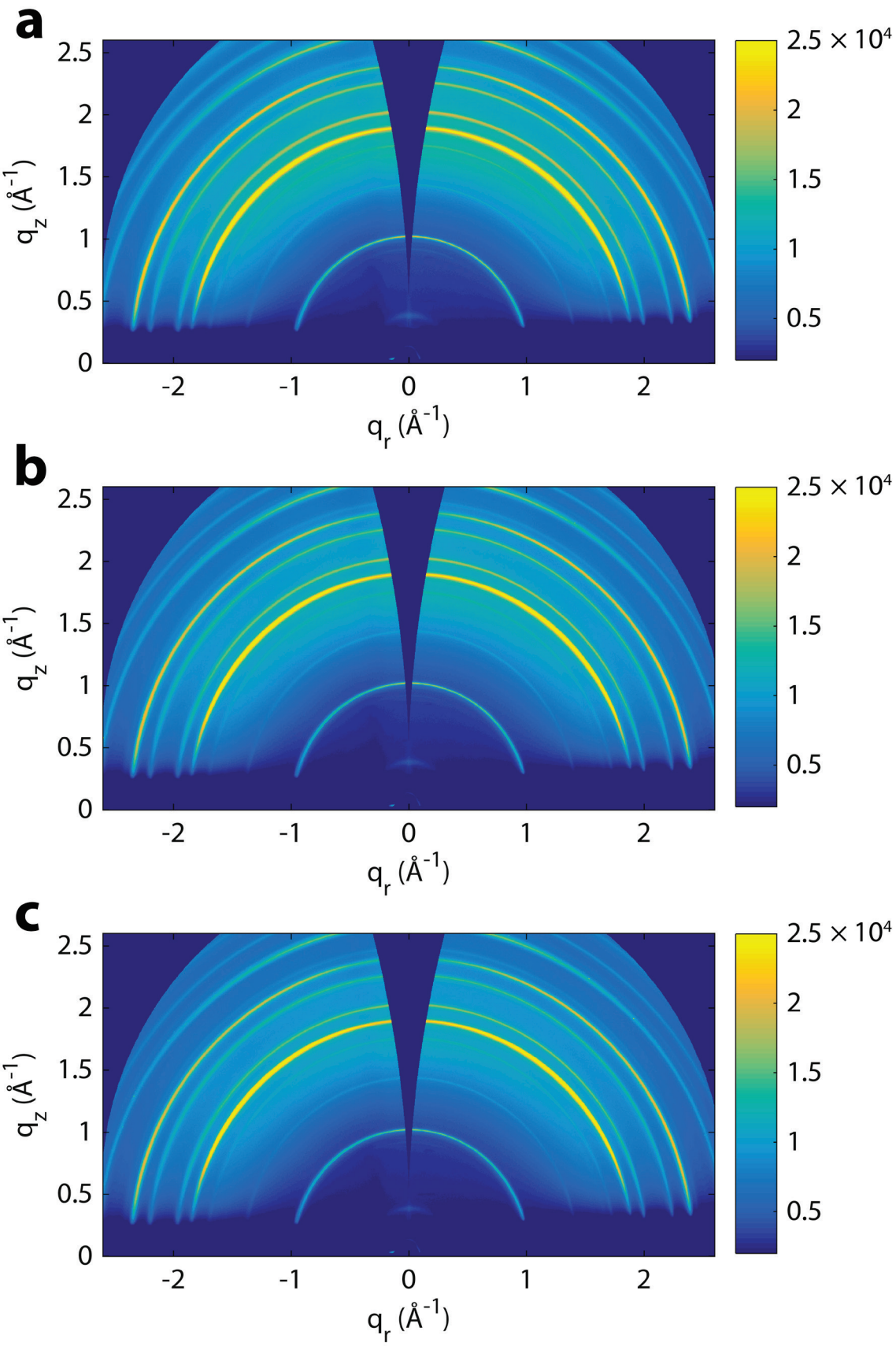

Figure S3. 2D GIWAXS patterns of a ITO/ZnO/$CH_3NH_3PbI_3$/P3HT/Ag cell during exposure to a dry (RH = 0-5%) nitrogen environment: (a) t = 0 h, (b) t = 0.75 h, (c) t = 1.8 h.

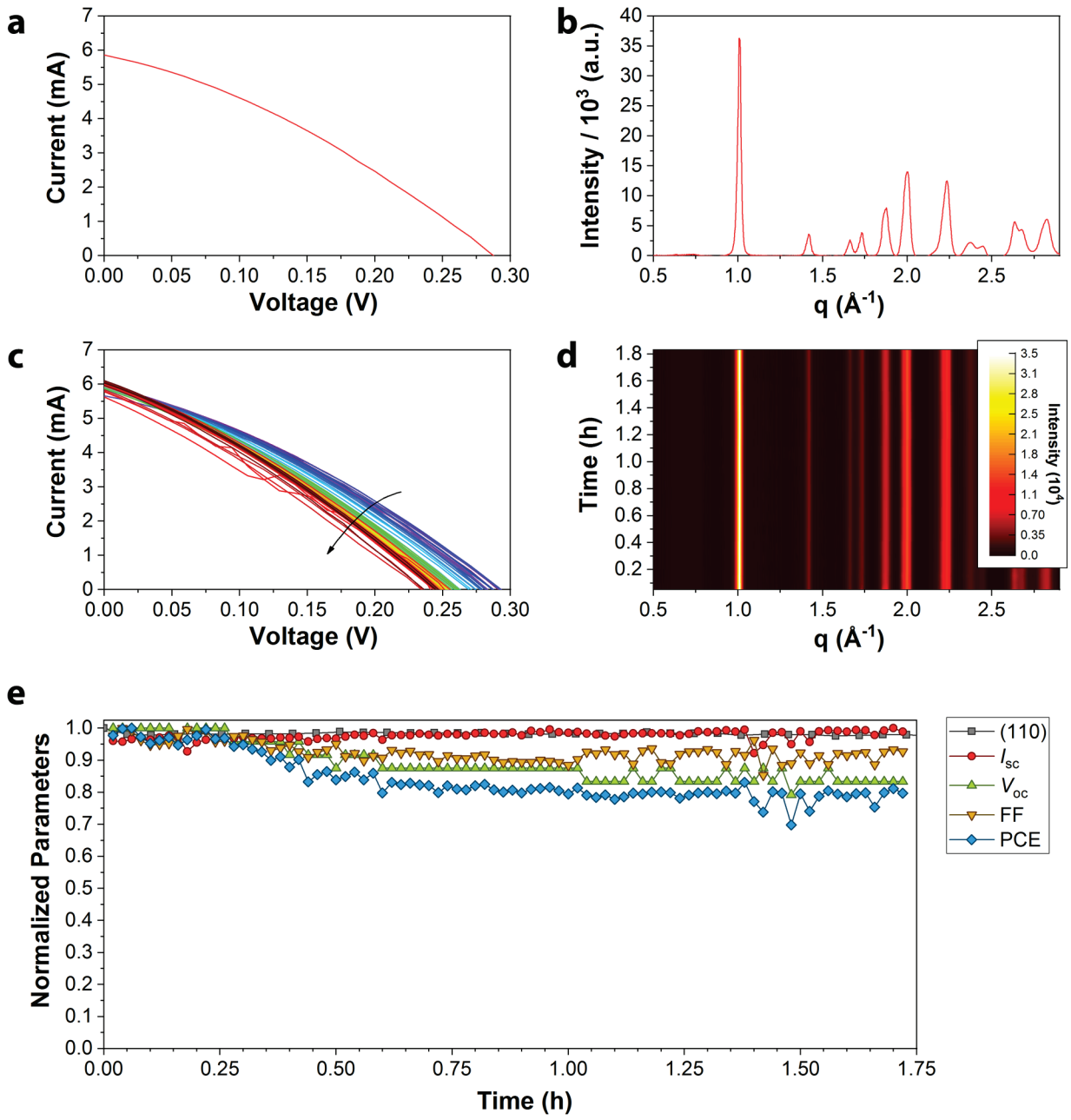

Figure S4. Initial (a) *I-V* curve and (b) azimuthally-integrated GIWAXS pattern for a ITO/ZnO/$CH_3NH_3PbI_3$/P3HT/Ag cell. (c) *I-V* curves acquired at 1 min intervals (t = 0 h, purple; t = 1.72 h, red) and (d) azimuthally-integrated GIWAXS patterns for the same cell after exposure to a dry (RH = 0-5%) nitrogen environment. (e) Normalized intensity of the (110) scattering peak and electrical device parameters over the course of the experiment.

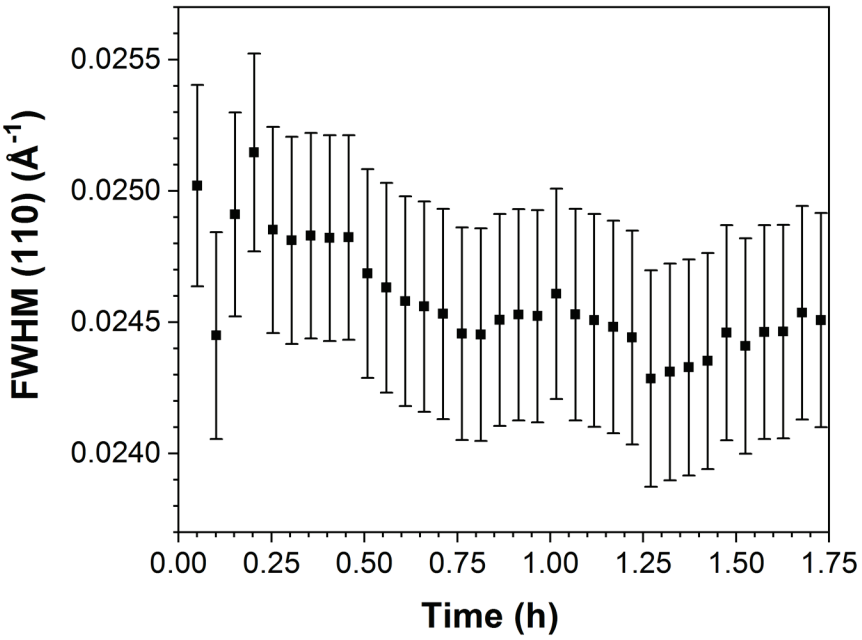

Figure S5. FWHM of the (110) scattering peak for a ITO/ZnO/$CH_3NH_3PbI_3$/P3HT/Ag cell after exposure to a dry (RH = 0-5%) nitrogen environment.

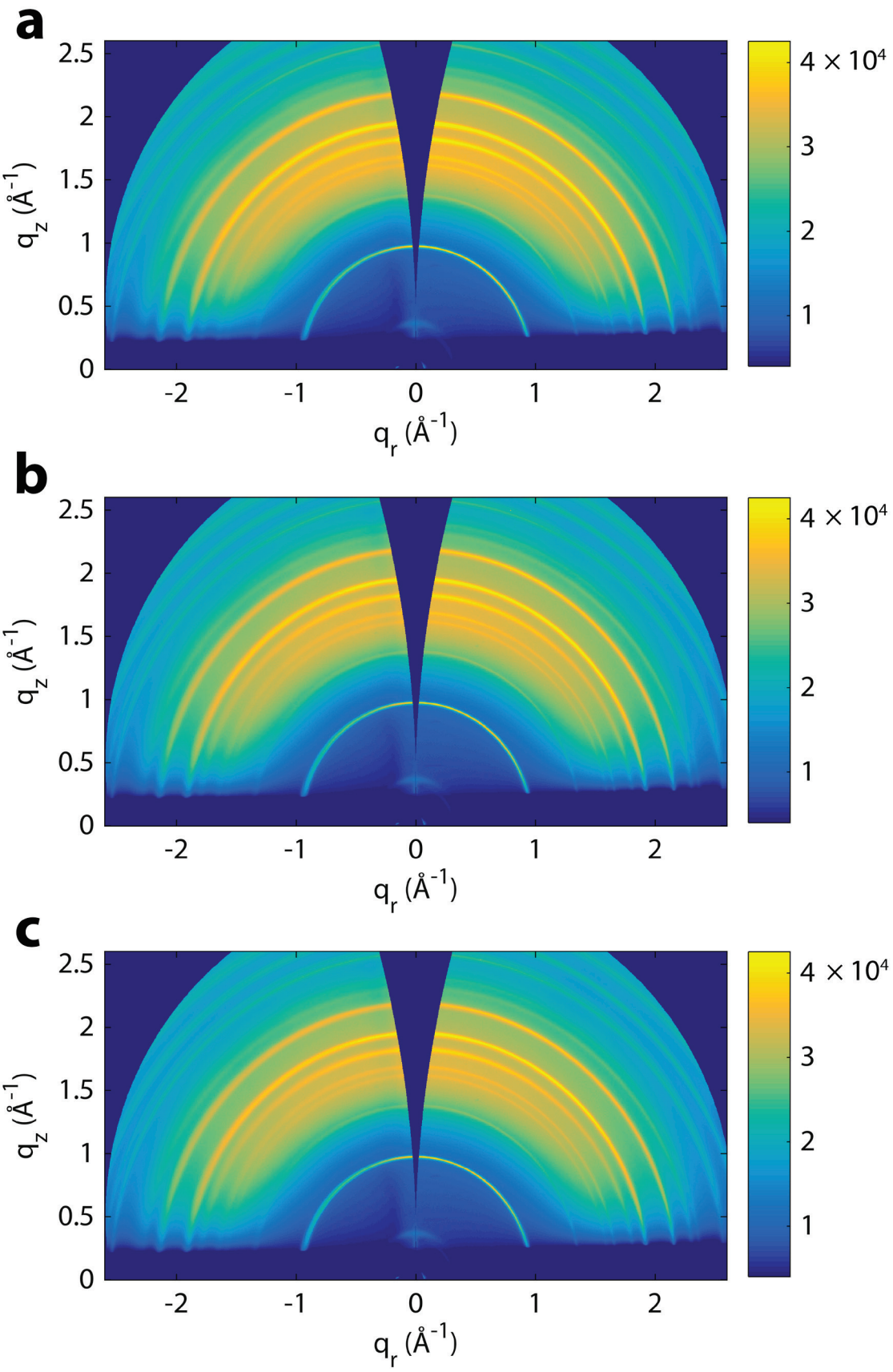

Figure S6. 2D GIWAXS patterns of a ITO/ZnO/$CH_3NH_3PbI_3$/P3HT/Ag cell during exposure to a humid (RH = 80%) nitrogen environment: (a) t = 0 h, (b) t = 0.85 h, (c) t = 1.6 h.

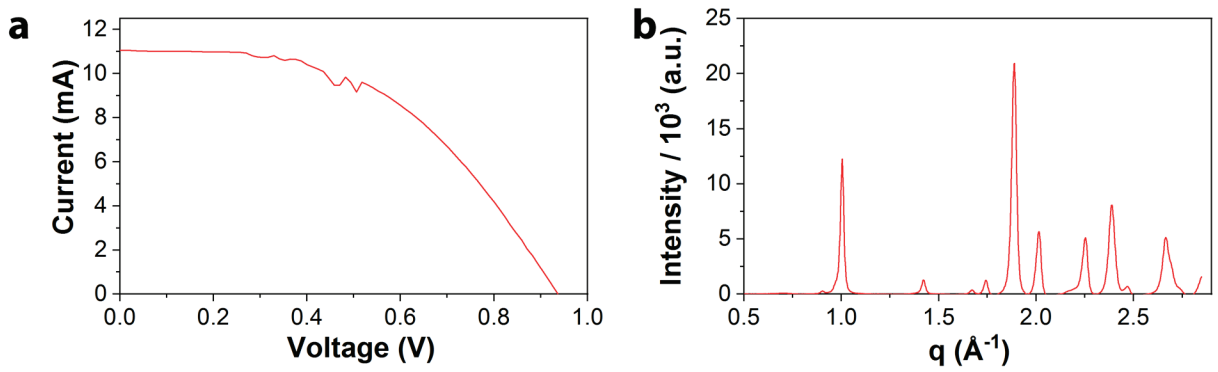

Figure S7. Initial (a) *I-V* curve and (b) azimuthally-integrated GIWAXS pattern for the ITO/ZnO/$CH_3NH_3PbI_3$/P3HT/Ag cell.

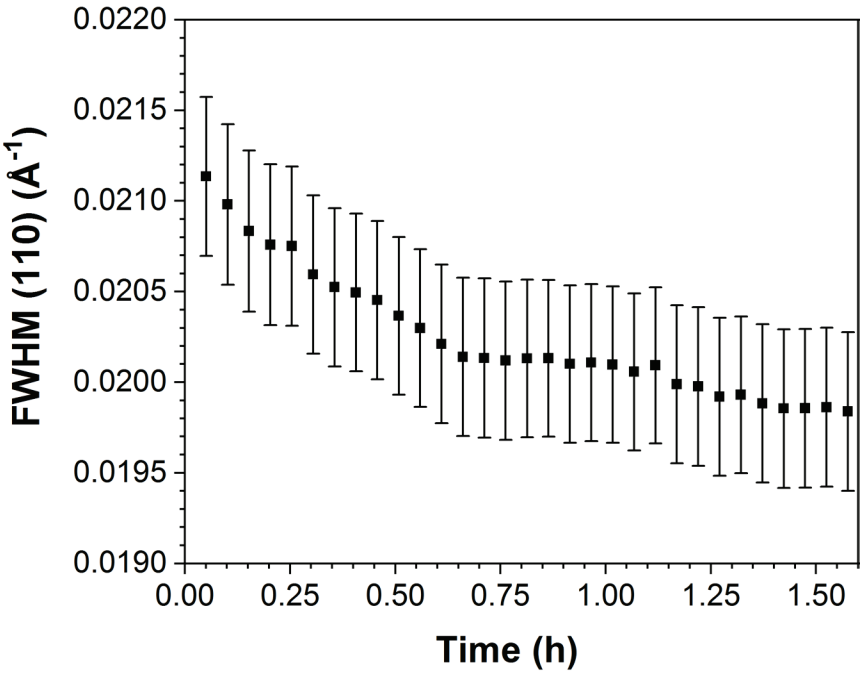

Figure S8. FWHM of the (110) scattering peak for a ITO/ZnO/$CH_3NH_3PbI_3$/P3HT/Ag cell after exposure to a humid (RH = 80%) nitrogen environment.

Table S2. Average device parameters for the FTO/ZnO/$CH_3NH_3PbI_3$/P3HT/Au cells prepared in this study.

J_{sc} (mA/cm^2)	V_{oc} (V)	FF	PCE (%)
14.4 ± 0.7	0.93 ± 0.02	0.61 ± 0.03	8.2 ± 0.4

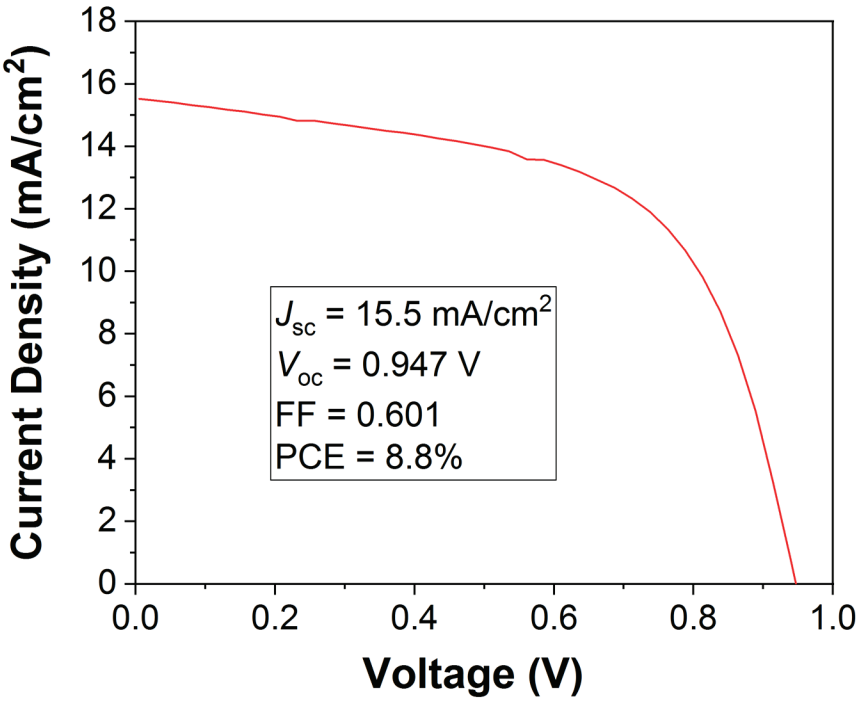

Figure S9. *J-V* curve of the champion FTO/ZnO/$CH_3NH_3PbI_3$/P3HT/Au cell from this study.

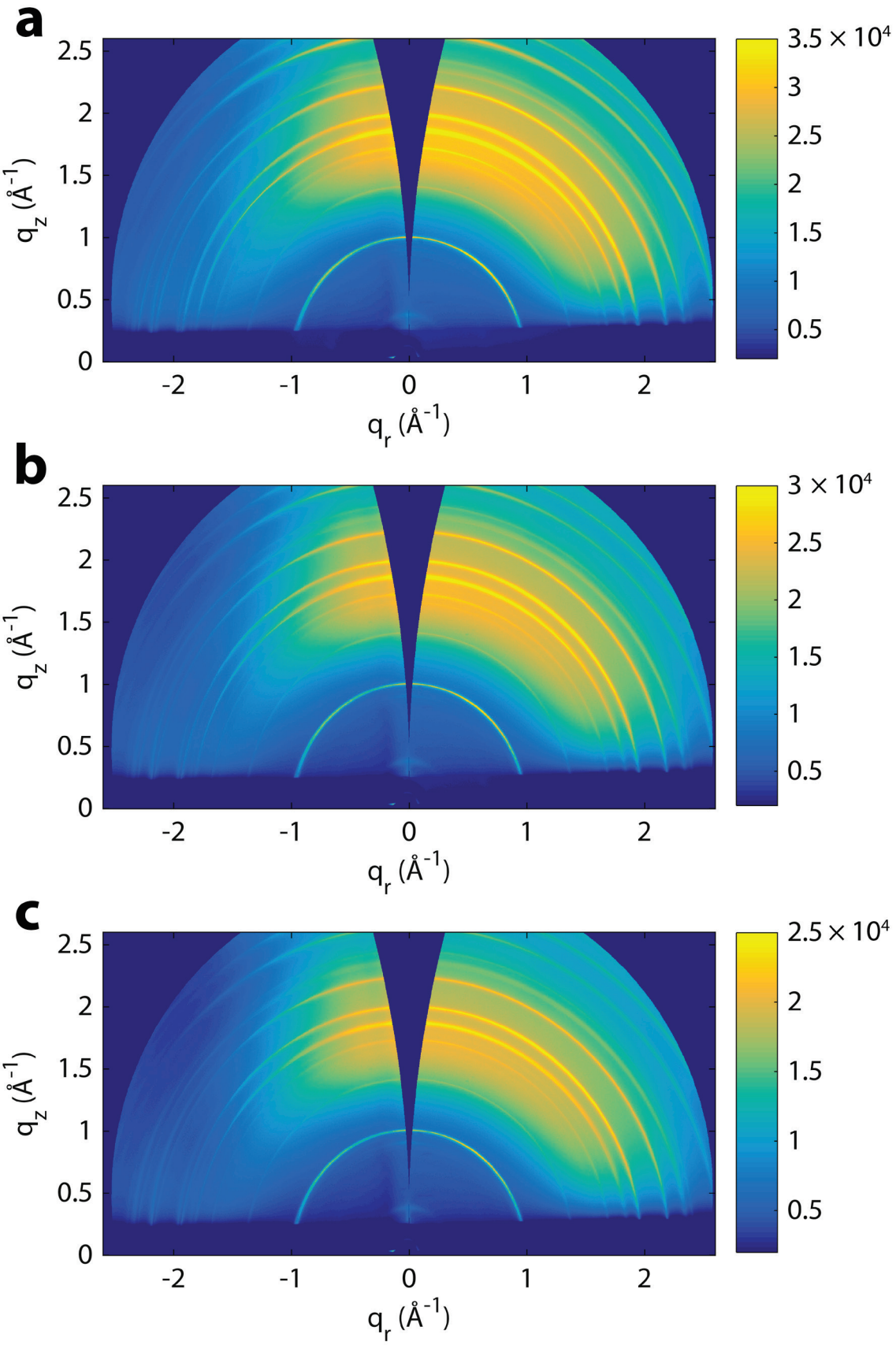

Figure S10. 2D GIWAXS patterns of a FTO/ZnO/$CH_3NH_3PbI_3$/P3HT/Au cell during exposure to a dry (RH = 0-5%) nitrogen environment: (a) t = 0 h, (b) t = 2.5 h, (c) t = 6 h.

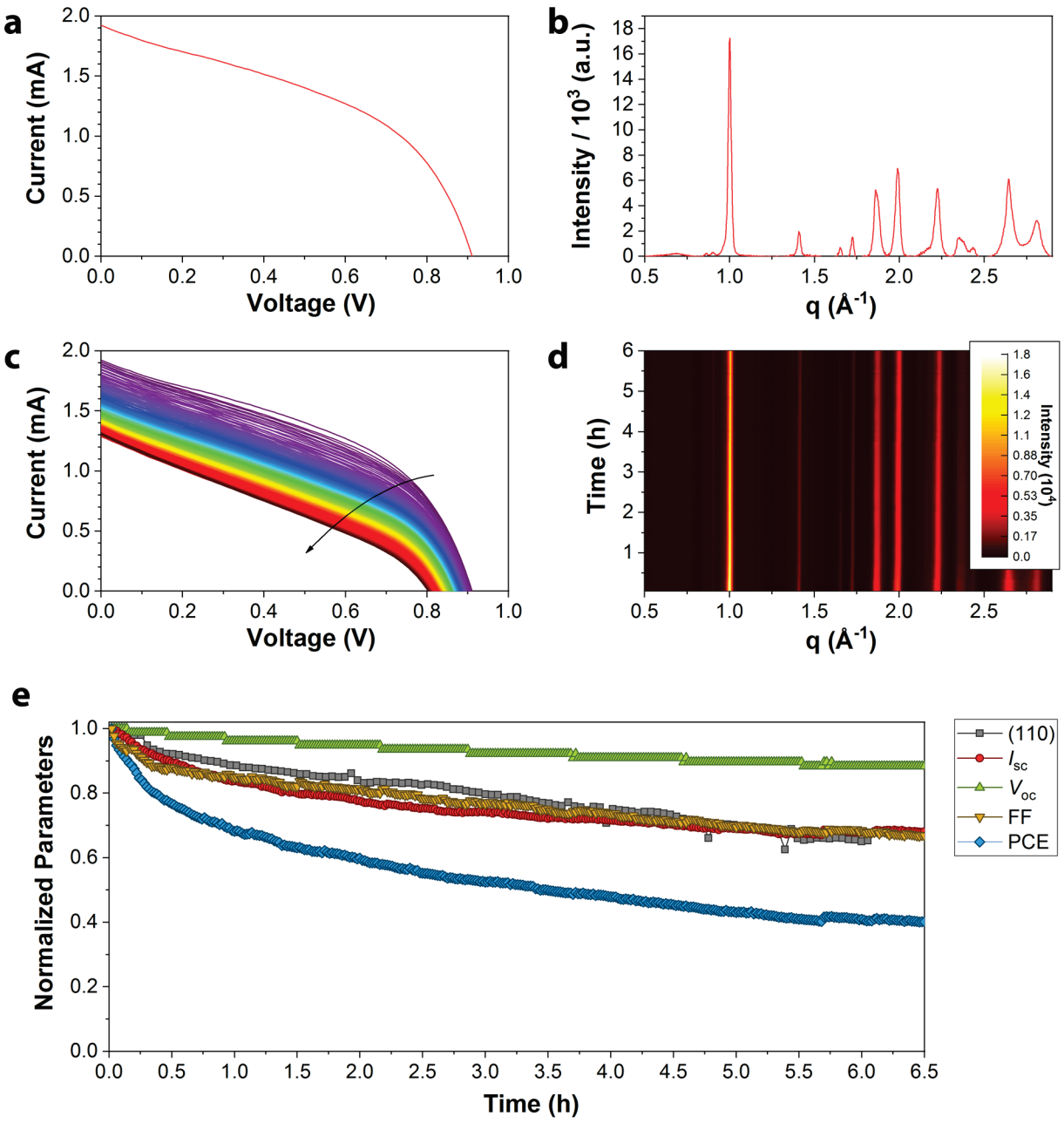

Figure S11. Initial (a) *I-V* curve and (b) azimuthally-integrated GIWAXS pattern for a FTO/ZnO/$CH_3NH_3PbI_3$/P3HT/Au cell. (c) *I-V* curves acquired at 1 min intervals (t = 0 h, purple; t = 6.5 h, red) and (d) azimuthally-integrated GIWAXS patterns for the same cell after exposure to a dry (RH = 0-5%) nitrogen environment. (e) Normalized intensity of the (110) scattering peak and electrical device parameters over the course of the experiment.

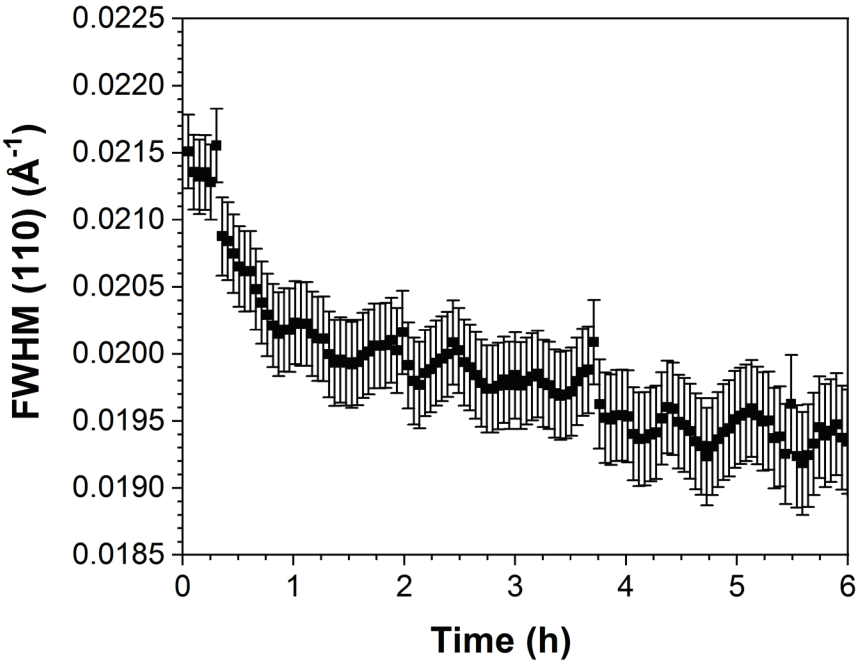

Figure S12. FWHM of the (110) scattering peak for a FTO/ZnO/$CH_3NH_3PbI_3$/P3HT/Au cell after exposure to a dry (RH = 0-5%) nitrogen environment.

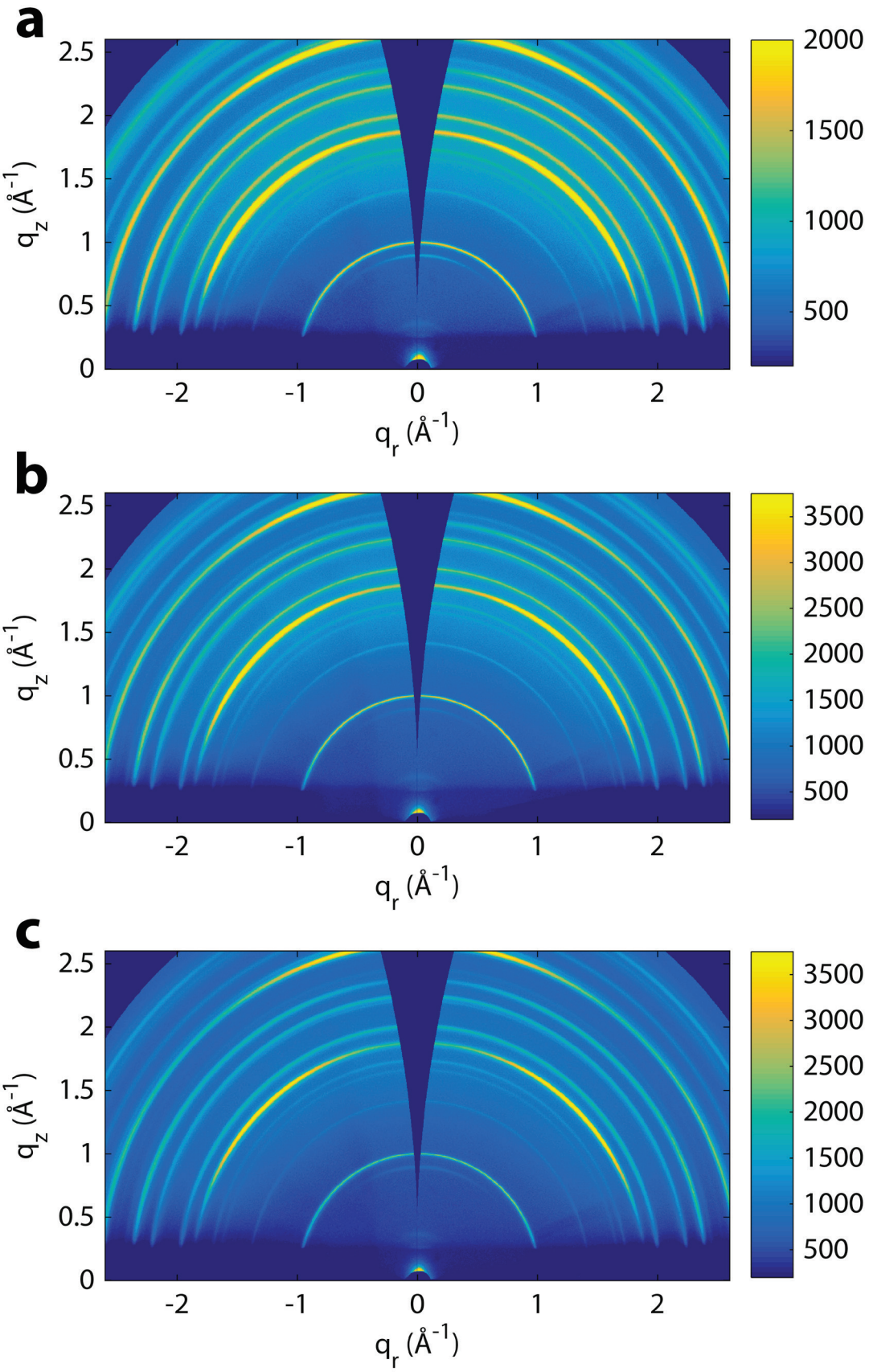

Figure S13. 2D GIWAXS patterns of a FTO/ZnO/$CH_3NH_3PbI_3$/P3HT/Au cell during exposure to a humid (RH = 85%) nitrogen environment: (a) t = 0 h, (b) t = 2.5 h, (c) t = 6 h.

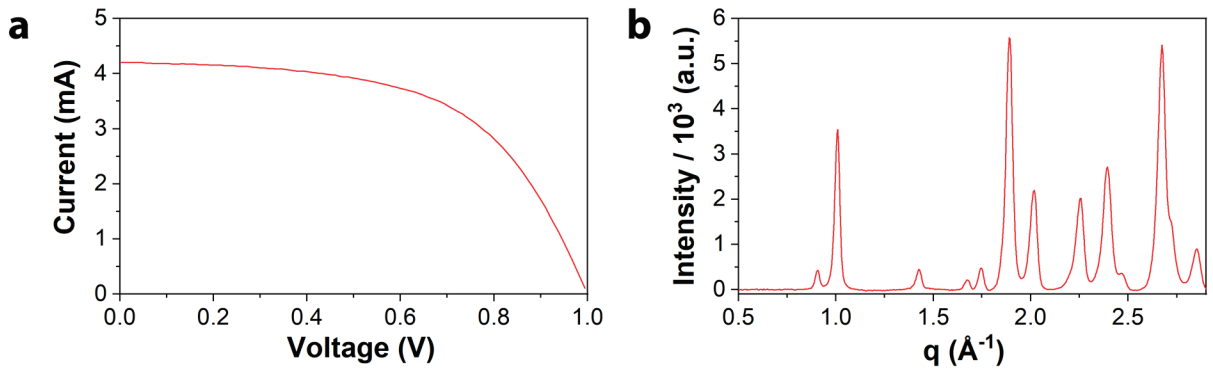

Figure S14. Initial (a) *I-V* curve and (b) azimuthally-integrated GIWAXS pattern for the FTO/ZnO/$CH_3NH_3PbI_3$/P3HT/Au cell.

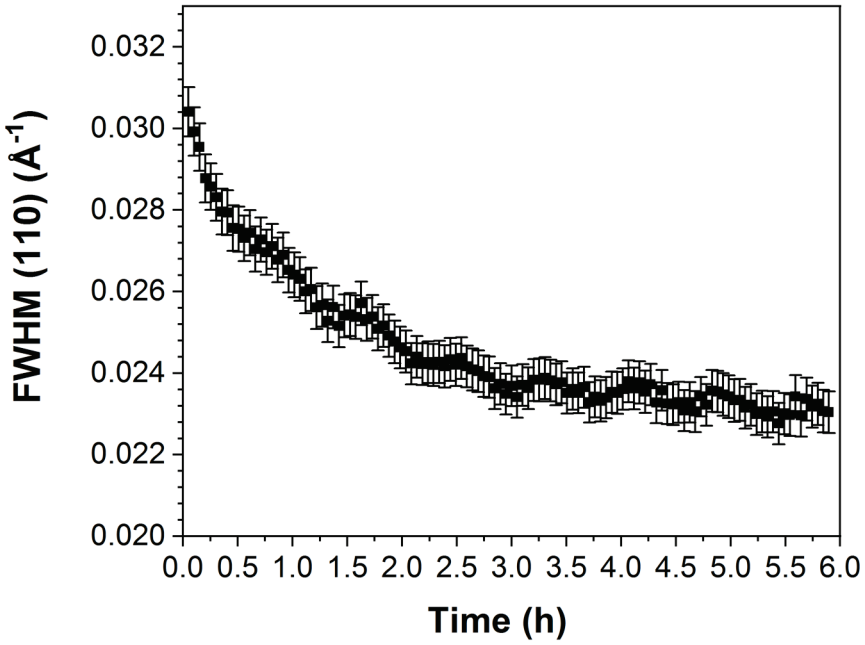

Figure S15. FWHM of the (110) scattering peak for a FTO/ZnO/$CH_3NH_3PbI_3$/P3HT/Ag cell after exposure to a humid (RH = 85%) nitrogen environment.

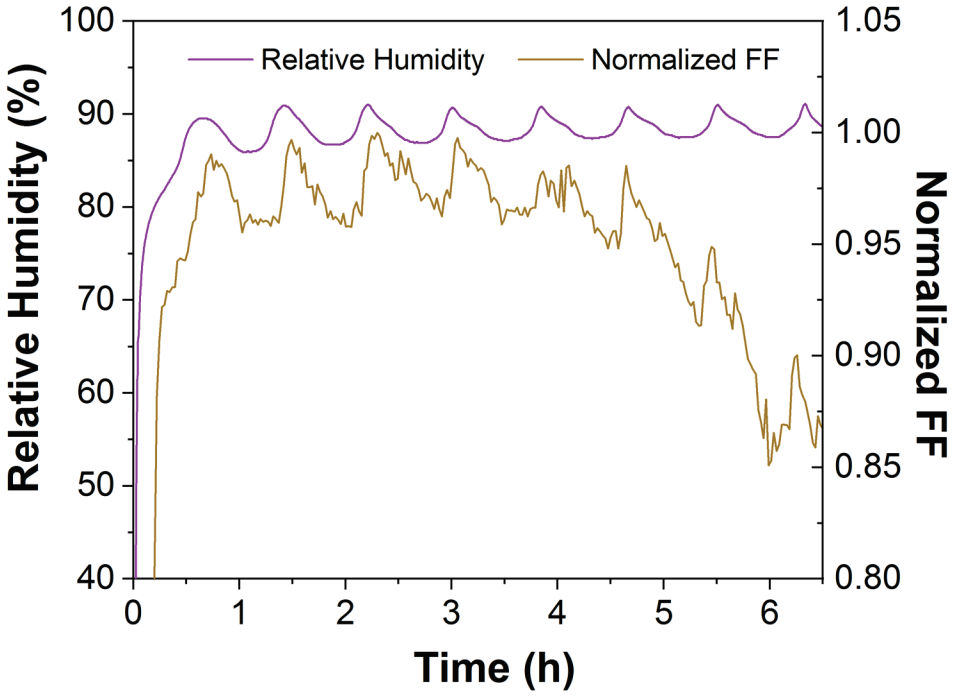

Figure S16. Relative humidity and normalized fill factor as a function of time for the FTO/ZnO/$CH_3NH_3PbI_3$/P3HT/Au cell.

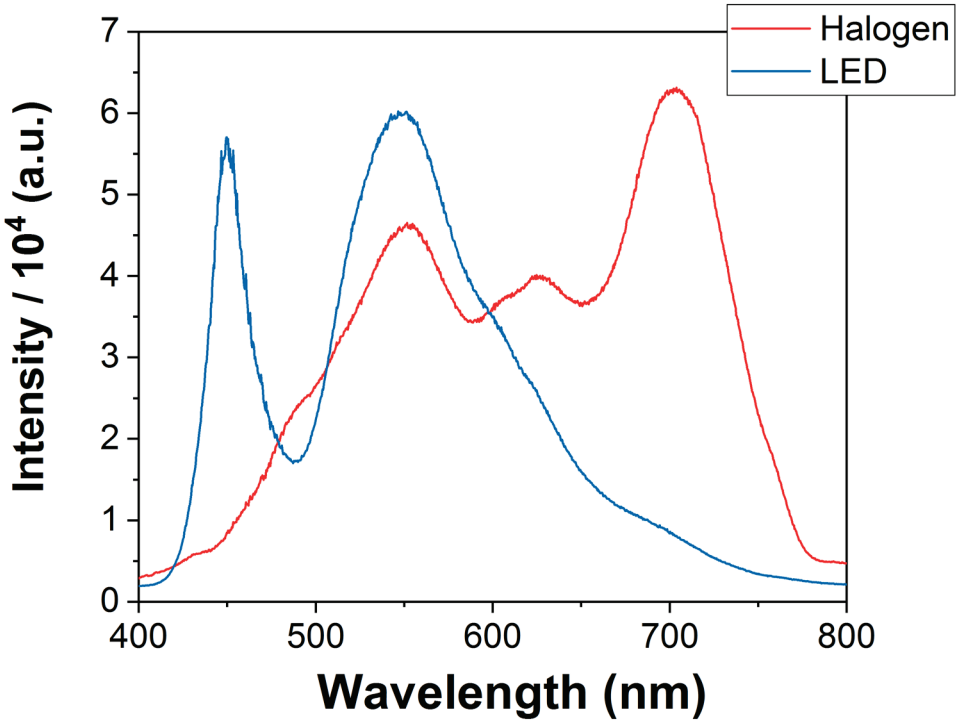

Figure S17. UV/vis emission spectra of the halogen and LED lightbulbs.

REFERENCES

(1) Lee, M. M.; Teuscher, J.; Miyasaka, T.; Murakami, T. N.; Snaith, H. J. Efficient Hybrid Solar Cells Based on Meso-Superstructured Organometal Halide Perovskites. *Science* **2012**, *338*, 643–647.

(2) Liu, D.; Kelly, T. L. Perovskite Solar Cells with a Planar Heterojunction Structure Prepared Using Room-Temperature Solution Processing Techniques. *Nat. Photonics* **2014**, *8*, 133–138.

(3) Gangishetty, M. K.; Scott, R. W. J.; Kelly, T. L. Effect of Relative Humidity on Crystal Growth, Device Performance and Hysteresis in Planar Heterojunction Perovskite Solar Cells. *Nanoscale* **2016**, *8*, 6300–6307.

(4) Jiang, Z. GIXSGUI: a MATLAB Toolbox for Grazing-Incidence X-ray Scattering Data Visualization and Reduction, and Indexing of Buried Three-Dimensional Periodic Nanostructured Films. *J. Appl. Cryst.* **2015**, *48*, 917-926.